A nuclear redox sensor modulates gene activation and *var* switching in *Plasmodium falciparum*

Adina Heinberg[a] , Inbar Amit-Avraham[a], Vera Mitesser[a] , Karina Simantov[a] , Manish Goyal[a] , Yuval Nevo[b], Sofia Kandelis-Shalev[a], Emilie Thompson[a], and Ron Dzikowski[a,1]

The virulence of *Plasmodium falciparum*, which causes the deadliest form of human malaria, is attributed to its ability to evade the human immune response. These parasites "choose" to express a single variant from a repertoire of surface antigens called PfEMP1, which are placed on the surface of the infected red cell. Immune evasion is achieved by switches in expression between *var* genes, each encoding a different *Pf*EMP1 variant. While the mechanisms that regulate mutually exclusive expression of *var* genes are still elusive, antisense long-noncoding RNAs (lncRNAs) transcribed from the intron of the active *var* gene were implicated in the "choice" of the single active *var* gene. Here, we show that this lncRNA colocalizes with the site of *var* mRNA transcription and is anchored to the *var* locus via DNA:RNA interactions. We define the *var* lncRNA interactome and identify a redox sensor, *P. falciparum* thioredoxin peroxidase I (*Pf*TPx-1), as one of the proteins associated with the *var* antisense lncRNA. We show that *Pf*TPx-1 localizes to a nuclear subcompartment associated with active transcription on the nuclear periphery, in ring-stage parasite, when *var* transcription occurs. In addition, *Pf*TPx-1 colocalizes with S-adenosylmethionine synthetase (*Pf*SAMS) in the nucleus, and its overexpression leads to activation of *var2csa*, similar to overexpression of *Pf*SAMS. Furthermore, we show that *Pf*TPx-1 knockdown alters the *var* switch rate as well as activation of additional gene subsets. Taken together, our data indicate that nuclear *Pf*TPx-1 plays a role in gene activation possibly by providing a redox-controlled nuclear microenvironment ideal for active transcription.

malaria | *Plasmodium falciparum* | var genes | lncRNA | thioredoxin peroxidase

Malaria remains a serious global health issue with 241 million cases and an estimated 627,000 deaths per year (1), mostly caused by the protozoan parasite, *Plasmodium falciparum*. The virulence of *P. falciparum* is attributed to its ability to modify the infected red blood cells (iRBCs), causing them to adhere to endothelial receptors, thereby removing the iRBCs from the circulation and preventing their clearance by the spleen and at the same time causing local inflammation and blockage of blood vessels. The major ligand responsible for the cytoadhesive properties of the iRBCs is *P. falciparum* erythrocyte membrane protein 1 (*Pf*EMP1), which is expressed by the parasite, placed on the iRBC surface, and binds to host endothelial receptors. *Pf*EMP1 is encoded by a multicopy gene family named *var*. Each *var* gene encodes a different *Pf*EMP1 variant, and the *var* gene repertoire in different parasite isolates may vary between 47 and 90 genes per parasite genome (2). To avoid unnecessary exposure of its antigenic repertoire, *var* gene expression has evolved so that each parasite expresses a single *var* gene at a time and maintains the rest of the gene family transcriptionally silent. Once the human immune system recognizes *Pf*EMP1, antibodies are generated to target the invading pathogen and often significantly reduce the number of infected cells. However, a small subset of parasites switches expression to a different *Pf*EMP1 variant, thereby avoiding antibody recognition and continuing the infection. Thus, the ability of the parasite to evade the antibody-mediated response against *Pf*EMP1 relies on mutually exclusive *var* gene expression and antigenic switches in expression between different *var* genes.

The mechanism of mutually exclusive *var* gene expression in human infections is not completely understood; however, it is epigenetically regulated and involves histone modifications, promoter pairing, and long-noncoding RNAs (lncRNAs) (3). The promoter found within the *var* intron is bidirectional and is responsible for the production of long-noncoding transcripts, which are capped but not polyadenylated (4), suggesting that they are retained and function in the nucleus. The antisense lncRNA is transcribed by the single active *var* gene at the ring stage when the *var* mRNA is produced. Ectopic expression of *var*-specific antisense lncRNAs activates a silent gene in a dose-dependent manner, while interference with the endogenous lncRNA leads to transcriptional down-regulation of the active *var* gene, switching, and loss of epigenetic memory (5).

Significance

The molecular mechanisms that regulate the "choice" for singular gene activation among multicopy gene families remains an unsolved mystery in eukaryotic gene expression. Immune evasion of *Plasmodium falciparum*, the parasite responsible for the deadliest form of human malaria, depends on its ability to switch between variable surface antigens, expressed in a mutually exclusive manner by the *var* gene family. We found that long-noncoding RNAs that mark the single active *var* gene are associated with redox sensor, *Pf* TPx-1, at the site of active transcription, in close proximity to the enzyme responsible for providing methyl groups for epigenetic memory. We demonstrate that *Pf* TPx-1 plays a pivotal role in *var* gene expression, possibly by providing optimal conditions for their epigenetic regulation.

However, the mechanism by which the lncRNA facilitates *var* gene activation is not understood. In other organisms, lncRNAs are implicated in recruitment of protein complexes important for chromatin modifications and transcriptional control (6). We hypothesized that the *var* antisense lncRNA could similarly function to recruit factors important for *var* expression.

We uncovered the antisense lncRNA interactome, which includes thioredoxin peroxidase I (*Pf*TPx-1), a well-studied redox protein that is responsible for H_2O_2 homeostasis and redox relays to downstream proteins (7–14). During the intraerythrocytic developmental cycle, the parasite is under constant oxidative stress from both inside and outside the RBC. As the parasite matures, it produces reactive oxygen species (ROS) from mitochondrial electron transport and from digestion of hemoglobin as a food source (15, 16). The parasite also encounters high levels of ROS from antimalarial compounds, high fevers, and immune cells. However, little is known about redox sensing and regulation of gene expression in *P. falciparum*. We found that in addition to its cytoplasmic role, *Pf*TPx-1 is also located in a subcellular nuclear compartment of active transcription that includes the *var* expression site. Furthermore, alterations in *Pf*TPx-1 expression change *var* gene switching and influence transcriptional activation of additional gene subsets. Taken together, these results demonstrate a role for *Pf*TPx-1 in gene regulation at a particular subnuclear compartment, potentially by creating an optimal niche for transcription.

Results

var Antisense lncRNAs Colocalize with the Site of *var* mRNA Transcription and Are Anchored via DNA:RNA Interactions.
We have previously shown that the antisense lncRNA is expressed from the promoter found within the intron of the active *var* gene (5). This lncRNA is incorporated into the chromatin and plays an important role in the activation of the single *var* gene that is expressed (5). To localize the antisense lncRNA transcript within the parasite nucleus, we performed two-color RNA-fluorescence in situ hybridization (FISH) with strand-specific RNA probes in the DC-J transgenic parasite line (17). This line allows for activation of a specific *var* gene (PF3D7_0223500-BSD) by culturing the parasites in the presence of blasticidin-S-HCl (DC-J "ON"), whereas a clonal parasite population grown in the absence of blasticidin (DC-J "OFF") expresses the PF3D7_0421300 *var* gene. Previous work showed that *var* transcripts localize to a specific nuclear site, which is distinct from the location of transcripts of unrelated genes (18). We observed colocalization of the *var* mRNA and antisense lncRNA at the nuclear periphery during the ring stage in both parasite populations (DC-J ON and OFF), indicating that the lncRNA is found in close proximity to the nascent *var* mRNA at the *var* expression site (Fig. 1 *A* and *B*). The vast majority of the signals observed were characteristically condensed spots with fewer than 5% showing a diffused pattern (Fig. 1*C*). However, when performing similar RNA-FISH using RNase H treatment to break up DNA:RNA hybrids, we found that 100% of the antisense lncRNA signals became diffused, while the majority of the *var* mRNA signals remained in condensed spots (Fig. 1 *D–F*). This result supports the idea that the antisense lncRNA is anchored to the *var* expression site via DNA:RNA interaction, possibly labeling the active locus.

The Conserved Region of the *var* Antisense lncRNA Is Predicted to Form Secondary RNA Structures.
The antisense lncRNA transcribed by *var* introns is 1.7- to 2.5-kb long and contains sequences from the intron as well as the 3′ region of exon 1 (4) (Fig. 2*A*). The intronic part of the RNA transcript is conserved among the *var* gene family and contains the sequence of the pairing elements, which were shown to be essential for *var* gene silencing and mutually exclusive expression (19). On the other hand, the transcript encoded by the 3′ of exon 1 contains hypervariable sequences that may contribute to the "choice" for specific *var* gene activation. We hypothesized that the *var* antisense lncRNA may contribute to *var* gene activation by forming a DNA:RNA hybrid with its gene-specific sequence and by recruiting activation factors to the "chosen" locus through its conserved region. Using a bioinformatic tool for structural RNA prediction (RNAalifold Server of the ViennaRNA WEB), we analyzed the antisense lncRNA conserved region from the entire *var* gene family. As expected, given its sequence conservation, the analysis revealed a unique secondary structure composed of a loop and a highly preserved stem at the first 20 nt, which contains a repetitive TATA sequence (4) (Fig. 2*B*, green). This basic structure of the loop and the conserved stem is maintained among all *var* genes, even though the number of stems vary (*SI Appendix*, Fig. S1).

The Conserved Region of *var* Antisense lncRNA Binds Specific Nuclear Proteins.
As a first step to identify the nuclear proteins that are recruited to the active *var* gene via the antisense lncRNA, we used biotinylated RNA probes specific to either the UA-RNA stem-loop (TATA) region or to the pairing element sequences (IntPE) of the conserved region of the antisense lncRNA of PF3D7_0223500 (Fig. 2*B* and *SI Appendix*, Table S1). A non-*Plasmodium* RNA sequence (HSL RNA) was used as a control. These probes were incubated with nuclear extract taken from ring-stage parasites (Fig. 2*C*). Identification of bound proteins by liquid chromatography tandem mass spectrometry (LC-MS/MS) revealed 33 and 39 proteins that were exclusively bound, or enriched more than 10-fold, to the TATA and PE probes, respectively (*SI Appendix*, Table S2 and S3). Interestingly, 28 proteins were shared between the two experiments, and among them are proteins involved in DNA:RNA binding, cellular metabolism, and translation (Table 1). To confirm that the proteins identified in the in vitro pull-down are present at the active *var* locus in cultured parasites, we performed domain-specific chromatin isolation by RNA purification, (dChIRP) (20, 21). RNA probes were designed for the conserved-intron region (P1), the hypervariable region (P2), and the 5′ region of exon 1 (P3), a region that does not have a complementary antisense transcript associated with it (Fig. 2*D* and *SI Appendix*, Table S4). It is worth noting that in this experiment, the variable P2 region is much larger than the conserved P1 region (206 bp vs. 1,663 bp). Nevertheless, P1 pulled down more proteins than P2 (55 vs. 19), and most of the P2-associated proteins were histones. These results support our hypothesis that P1 might be involved in recruiting proteins to the active *var* gene locus. We identified 28 proteins that were uniquely associated with the conserved P1 domain of the antisense lncRNA (Fig. 2*E* and *SI Appendix*, Tables S5 and S6). To narrow down our analysis, we looked at the overlap between the proteins identified by all three approaches and found three proteins: thioredoxin peroxidase I (*Pf*TPx-1, PF3D7_1438900), ornithine aminotransferase (*Pf*OAT, PF3D7_0608800), and elongation factor 2 (PF3D7_1451100) (Table 1, boldface). Given the reasons below, we chose to focus on *Pf*TPx-1.

Pf TPx-1 Is Localized to the Active *var* Expression Site in Ring-Stage Parasites.
*Pf*TPx-1 belongs to the 2-Cys peroxiredoxin family that is responsible for detoxifying ROS and reactive nitrogen
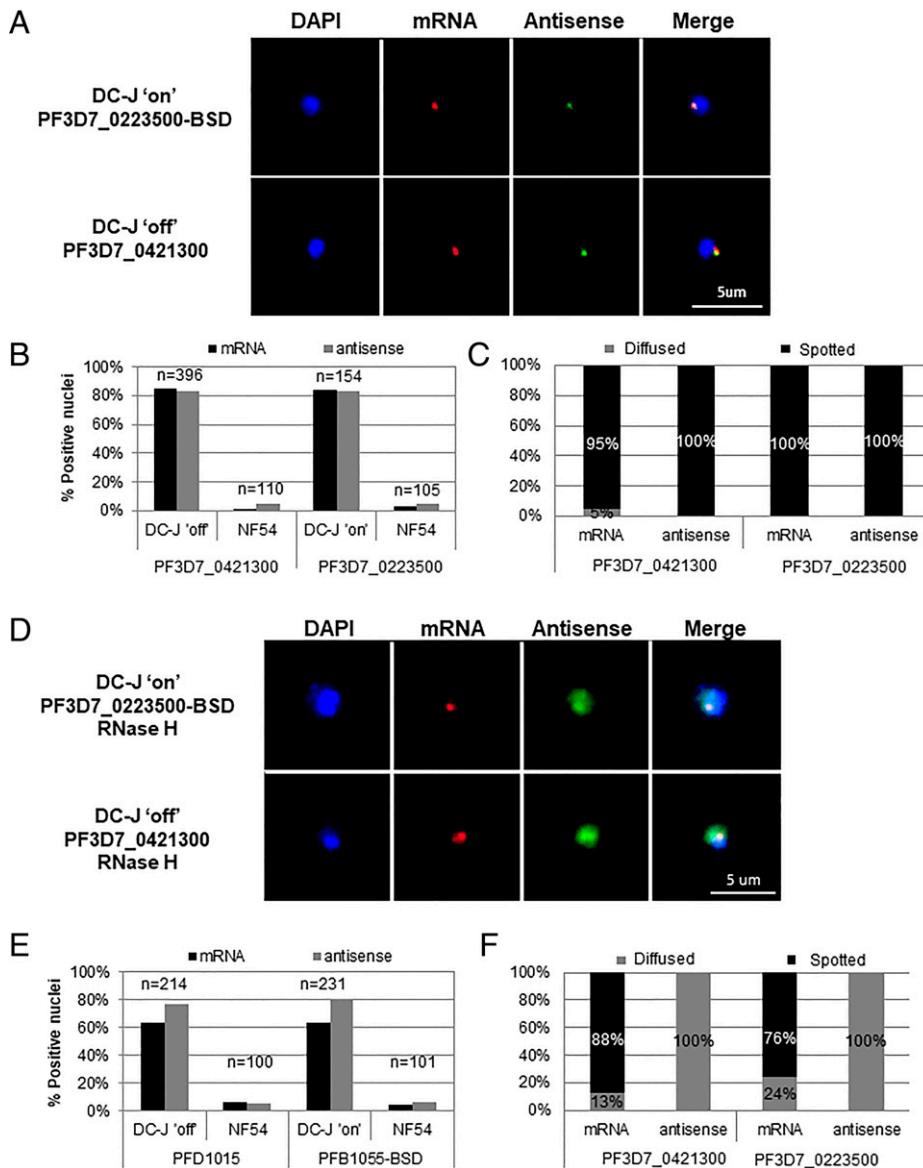
Fig. 1. *var* antisense lncRNAs colocalize with the site of *var* mRNA transcription and are anchored via DNA:RNA interactions. Dual color RNA-FISH of the *var* antisense lncRNA and the *var* mRNA of two different active *var* genes in tightly synchronized ring stage parasites at ~18 h postinvasion. Nuclei are stained with DAPI (blue). (*A*) Dual color RNA-FISH showing the nuclear positioning of messenger RNA (red) and antisense ncRNA (green) actively transcribed from the PF3D7_0223500-BSD (*Upper*) or PF3D7_0421300 (*Lower*) *var* genes. (*B*) Quantification of positive nuclei shown in *A*. (*C*) Quantification of fluorescent signal appearance (diffused vs. spotted) of positive nuclei shown in *A*. (*D*) Nuclear positioning of mRNA (red) and antisense ncRNA (green) actively transcribed from the PF3D7_0223500-BSD (*Upper*) or PF3D7_0421300 (*Lower*) *var* genes after treatment with 120U of RNase-H. (*E*) Quantification of positive nuclei shown in *D*. (*F*) Quantification of fluorescent signal appearance (diffused vs. spotted) of positive nuclei shown in *D*. (Scale bars, 5 μm.)

species from the parasite's oxygen-rich environment (14). In addition to their peroxidase activity, peroxiredoxins are now recognized as sensors and transducers of H_2O_2 status via the transfer of their oxidation state to effector proteins (22). *Plasmodium* parasites possess five peroxiredoxins localizing to various organelles, including the nucleus, cytoplasm, and mitochondria (23). *Pf*TPx-1 is abundantly expressed in the trophozoite stage and is described as a cytoplasmic protein (7). We were intrigued that we repeatedly identified *Pf*TPx-1 as a nuclear protein associated with the lncRNA transcribed by the active *var* gene, and decided to further investigate the nuclear role of *Pf*TPx-1, specifically looking at *var* gene regulation. As a first step, we created a recombinant *Pf*TPx-1 and confirmed its ability to directly bind the *var* antisense lncRNA by RNA EMSA (*SI Appendix*, Fig. S2).

We then created a transgenic line using the selection-linked integration (pSLI) system (24), where *Pf*TPx-1 was endogenously tagged with 3× HA-tags and the *glmS* ribozyme was fused with the mRNA transcript to allow for inducible knockdown of the gene upon the addition of glucosamine (25) (*SI Appendix*, Fig. S3). Immunofluorescence analysis (IFA) revealed that *Pf*TPx-1 localizes to a distinct focus at the nuclear periphery in ring-stage parasites and is more diffused in late stages (Fig. 3*A* and *SI Appendix*, Fig. S4). Using superresolution

stochastic optical reconstruction microscopy (STORM) imaging, we were able to visualize the nuclear signal at higher resolution and obtained two patterns of localization: one in which the *Pf*TPx-1 signal is clustered to one concentrated spot on the nuclear periphery (Fig. 3 *B*, *Left*), and another where the signal is in patches along one side of the nuclear periphery (Fig. 3 *B*, *Right*). While this difference is likely due to differences in orientation of the parasite, it seems that *Pf*TPx-1 occupies a larger nuclear region than just the *var* expression site. To confirm that *Pf*TPx-1 is indeed nuclear in ring-stage parasites, we performed subcellular fractionation and detected *Pf*TPx-1 in both nuclear and cytoplasmic compartments in ring-stage parasites, while in later stages it is mostly cytoplasmic (Fig. 3*C*). This is in agreement with a previous proteomic analysis that also found *Pf*TPx-1 in the nucleus (26). To determine whether the nuclear *Pf*TPx-1 observed in ring-stage parasites localizes to the *var* expression site, we performed RNA-FISH in parasites exclusively expressing *var2csa* (CSA line). We visualized the active *var* gene using *var2csa*-specific probes and observed colocalization of *Pf*TPx-1 with the *var* mRNA signal in all the cells where both signals were present ($n = 111$), confirming the results of our pull-down experiments that *Pf*TPx-1 is found at the *var* expression site (Fig. 3*D* and *SI Appendix*, Fig. S5).
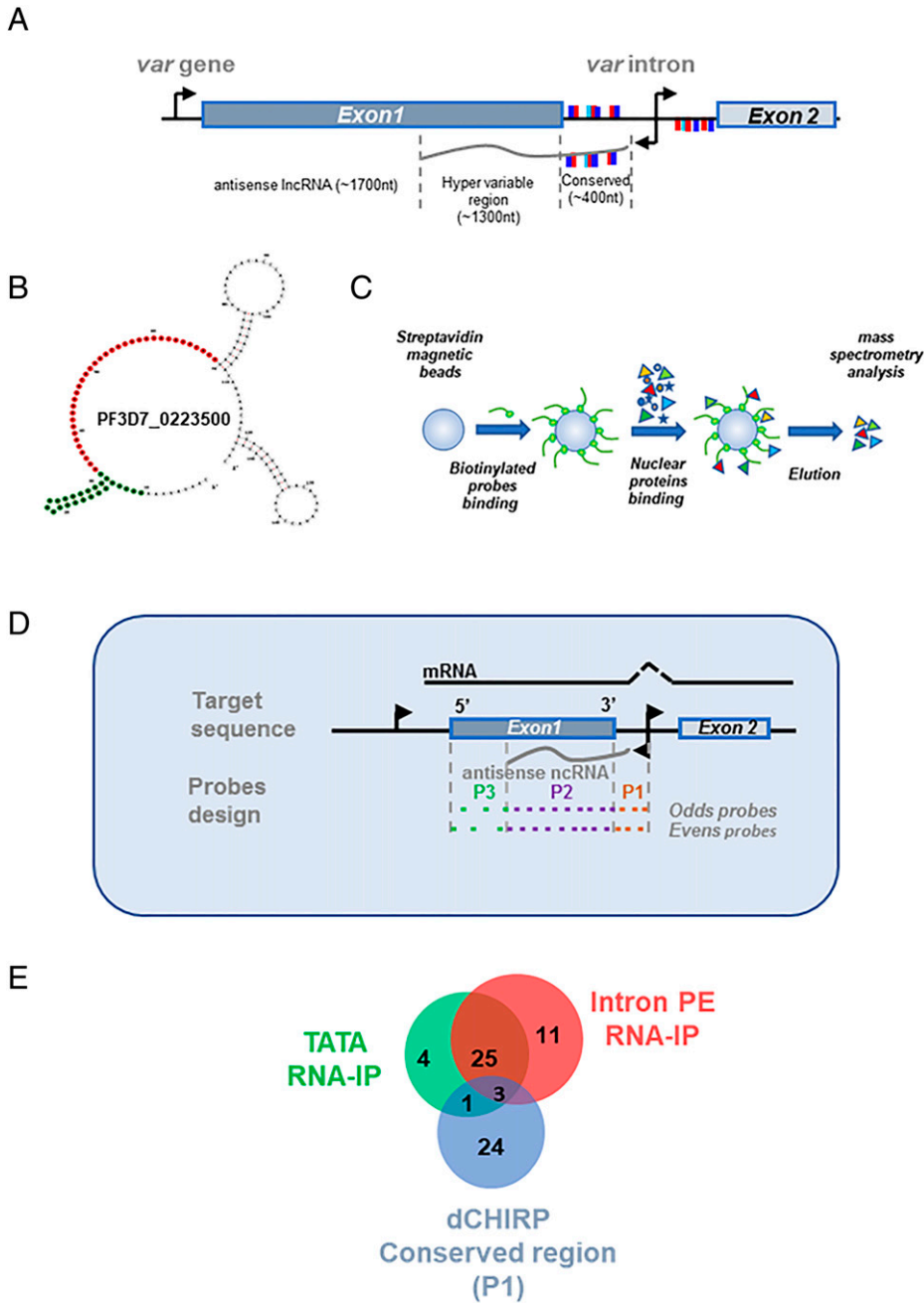
Fig. 2. The conserved region of the *var* antisense lncRNA is predicted to form secondary RNA structure and binds specific nuclear proteins. (*A*) Schematic diagram of *var* gene structure. The antisense lncRNA (gray line, ~1.7 kb in length) is transcribed from a bidirectional promoter located at the *var* intron (black arrows) and can be divided into two regions: conserved region complimentary to the *var* intron (~400 nt in length) and a hypervariable region complimentary to exon 1 (~1,300 nt in length). The pairing element (PE) repeats of the *var* intron are marked with light blue, dark blue, and red rectangles. The presentation of the PE motifs above or below the genes represents their orientation on the DNA strands and on the lncRNA. (*B*) Secondary structure of PF3D7_0223500-BSD *var* antisense conserved region. Positions marked in green served for the antisense UA-RNA stem-loop probe (TATA) and positions marked in red served for the antisense PE RNA probe (IntPE). Prediction of secondary structures was done using the RNAfold Server of the ViennaRNA WEB. (*C*) Schematic diagram of affinity chromatography assay using streptavidin coated magnetic beads (blue circle), biotinylated nucleic acid probes (green circle and orange line, respectively), and nuclear extract (colored shapes). Purified proteins were analyzed using MS. Affinity chromatography was performed with nuclear extract produced from DC-J ON parasite line in which the chromosomal bsd cassette (PF3D7_0223500-BSD) is active. (*D*) dChIRP was performed using the DC-J OFF parasite line in which the *var* gene, PF3D7_0421300, is active. Two sets of probes were designed to bind the antisense lncRNA of PF3D7_0421300 (odds and evens) and were divided to three pools; probes designed to bind the conserved region of the antisense lncRNA (P1), probes designed to bind the hypervariable region of the antisense lncRNA (P2), and probes that are complementary to the 5′ edge of exon 1 in which the *var* lncRNA antisense does not reach (P3). Tightly synchronized ring-stage parasites at ~18 h postinvasion were cross-linked and sonicated. Biotinylated probes were incubated with parasite extract and were bound to streptavidin magnetic beads. Proteins bound in each pool were identified using LC-MS/MS. (*E*) Venn diagram depicting the overlap in proteins identified using the three experimental approaches: TATA-stem loop affinity chromatography, IntPE single-stranded RNA affinity chromatography, and dCHIRP.

Remarkably, while the signal of the *var2csa* transcript overlaps with *Pf*TPx-1 (Mander's overlap coefficient 0.97), the *Pf*TPx-1 signal occupies a larger nuclear area (Mander's overlap coefficient 0.34), indicating that *Pf*TPx-1 may have additional nuclear functions that are not limited to the *var* expression site.

PfTPx-1 Localizes to a Transcriptionally Active Nuclear Region in Ring-Stage Parasites. We were further interested in checking whether additional genes transcribed at a particular subnuclear compartment are associated with *Pf*TPx-1. One of the most abundant RNA species transcribed in ring-stage parasites are rRNAs located in a peri-nuclear compartment overlapping with the nucleolar marker fibrillarin (PF3D7_1407100), also referred to as *Pf*Nop1 (27). Although a defined nucleolus was never observed in *Plasmodium*, *Pf*TPx-1 has been shown to interact with *Pf*Nop1 in vitro (8, 10). Using IFA analysis, we found that in ring-stage parasites *Pf*TPx-1 and *Pf*Nop1 were adjacent at the nuclear periphery, with some regions of overlap

(Fig. 4*A*). Superresolution STORM imaging confirmed this observation and more clearly distinguished regions where the two proteins colocalized (Fig. 4*B*), indicating that *Pf*TPx-1 is also present in the area referred to as the nucleolus where active transcription of rDNA takes place. An additional subnuclear compartment associated with active transcription is the region near the nuclear pore complexes (NPC). Gene positioning near the NPC is thought to enhance transcription and aid in immediate mRNA transport (28, 29). *P. falciparum* shows a unique clustering of the NPC at a distinct region of the nuclear envelope in ring-stage parasites, as well as in late schizonts, where these clusters are located adjacent to euchromatic regions (30, 31). Given that *Pf*TPx-1 is present in a region of active transcription, we tested whether active transcription could take place near the NPC. We used *Pf*Sec13, which was shown to be an essential nucleoporin, as a marker for the NPC (30). We found that in ring-stage parasites, *Pf*TPx-1 colocalizes with *Pf*Sec13, with *Pf*TPx-1 once again occupying a larger region

Table 1. Nuclear proteins identified by affinity chromatography in both the TATA-stem loop and PE sequences of the antisense lncRNA

| Cellular process	PlasmoDB ID	Annotation	Enrichment	
			IntPE	TATA
DNA/RNA binding	PF3D7_0919000	Nucleosome assembly protein	*	*
	PF3D7_1006200	DNA/RNA-binding protein Alba 3	*	*
	PF3D7_1011800	PRE-binding protein	*	*
	PF3D7_1105100	Histone H2B	63-fold	55-fold
	PF3D7_1202900	High mobility group protein B1	*	*
	PF3D7_1224300	Polyadenylate-binding protein 1, putative	*	*
	PF3D7_1347500	DNA/RNA-binding protein Alba 4	*	*
	PF3D7_1426100	Transcription factor BTF3, putative	*	*
	PF3D7_1438900	**Thioredoxin peroxidase 1**	50-fold	42-fold
Metabolism	PF3D7_0513300	Purine nucleoside phosphorylase	*	*
	PF3D7_0608800	**Ornithine aminotransferase**	*	*
	PF3D7_0922500	Phosphoglycerate kinase	*	*
	PF3D7_1324900	L-lactate dehydrogenase	*	*
	PF3D7_1444800	Fructose-bisphosphate aldolase	*	*
	PF3D7_1462800	Glyceraldehyde-3-phosphate dehydrogenase	*	*
Translation	PF3D7_0309600	60S acidic ribosomal protein P2	*	*
	PF3D7_0517000	60S ribosomal protein L12, putative	*	*
	PF3D7_0913200	Elongation factor 1-β	*	*
	PF3D7_1357100	Elongation factor 1-α	22-fold	12-fold
	PF3D7_1451100	**Elongation factor 2**	*	*
Conserved unknown function	PF3D7_0721100	Conserved protein, unknown function	*	*
	PF3D7_0813300	Conserved protein, unknown function	*	*
	PF3D7_1115800	Conserved *Plasmodium* protein, unknown function	*	*
Other	PF3D7_0505800	Small ubiquitin-related modifier	*	*
	PF3D7_0826700	Receptor for activated c kinase	*	*
	PF3D7_1115600	Peptidyl-prolyl *cis-trans* isomerase	*	*
	PF3D7_1129100	Parasitophorous vacuolar protein 1	*	*
	PF3D7_1229400	Macrophage migration inhibitory factor	*	*

Proteins were grouped by function. The three proteins shaded in boldface were also identified using the dCHIRP methodology. A full list of proteins identified in each method can be found in *SI Appendix*, Tables S2, S3, S5, and S6. Asterisks (*) denotes proteins exclusively found in antisense specific versus control probes.

than *Pf* Sec13 (Fig. 4*C*). Furthermore, since we found that the active *var* gene colocalized with *Pf* TPx-1 (Fig. 3*D*), we tested the association of the *var* expression site and the NPC. We performed RNA-FISH in the *var2csa* expressing line, ectopically expressing a *Pf* Sec13-Halo fusion protein, and found that *Pf* Sec13 colocalizes with the active *var* gene in over 80% of the parasites (*n* = 128) (Fig. 4*D*). Altogether, these observations indicate that *Pf* TPx-1 is located in regions of active transcription near the NPC during the ring stage.

PfTPx-1 Is Involved in *var* Gene Switching. Given that *Pf* TPx-1 is found at the *var* expression site, we reasoned that altering expression of *Pf* TPx-1 may lead to changes in *var* gene expression. The *Pf* TPx-1_HAglmS transgenic line was created in the DC-J background to allow for selective activation of the *var-bsd* gene (PF3D7_0223500-BSD), which also enables controlled monitoring of *var* switching patterns over time upon *Pf* TPx-1 knockdown. We chose a clone in which the *var-bsd* transgene was silent and another *var* gene was active (PF3D7_1240300/ 1240600) (*SI Appendix*, Fig. S6*D*), and knocked down *Pf* TPx-1 expression using 5 mM GlcN (Fig. 5*A* and *SI Appendix*, Fig. S6*A*). We observed that upon the addition of blasticidin, RNA levels of the active *var* gene go down as the *var-bsd* transgene (PF3D7_0223500-BSD) becomes the dominant transcript in the parasite culture (Fig. 5*C* and *SI Appendix*, Fig. S8*B*), indicating that switching can occur despite *Pf* TPx-1 knockdown. We then removed blasticidin from the cultures and followed *var* switching patterns over time (Fig. 5*A*). We found that the switch

rate per generation in parasites in which *Pf* TPx-1 was knocked down by GlcN was reduced by 40 to 55% (1.2 to 1.26 off rate per generation) compared to the DC-J parent line where *Pf* TPx-1 is expressed and displayed a 2.1 to 2.7% off rate per generation (32) (Fig. 5*B*). *Pf* TPx-1_HAglmS parasites growing on regular media displayed a 15 to 41% reduction in switch rate (1.6 to 1.8 off rate per generation) compared to the parent line. Interestingly, we found that *Pf* TPx-1 expression levels, measured by RT-qPCR, were reduced in the *Pf* TPx-1_HAglmS transgenic line even without addition of GlcN (*SI Appendix*, Fig. S6*B*), which is associated with the reduction in *var* switch rate (Fig. 5*B*). In addition, we observed unusually high levels of the active *var* transcript in our *Pf* TPx-1_HAglmS transgenic line, where *Pf* TPx-1 transcription levels are low as compared to the DC-J control (*SI Appendix*, Figs. S6*B*, S7, and S8*A*). This increase in transcript abundance is even more pronounced upon *Pf* TPx-1 knockdown, suggesting that switching away from the active *var* gene is altered when *Pf* TPx-1 levels are low (*SI Appendix*, Fig. S7). Taken together, these data suggest that *var* gene switching is delayed without sufficient *Pf* TPx-1 expression.

Overexpression of PfTPx-1 Induces Switching to *var2csa*. As a complementary approach to *Pf* TPx-1 knockdown, we used a regulatable system (33) to overexpress *Pf* TPx-1 in an NF54 clonal population (C3) by increasing blasticidin concentrations (*SI Appendix*, Fig. S9*A*). To control for any off-target effects of blasticidin, a similar plasmid expressing GFP was transfected into the same parasite line. We monitored the expression of the
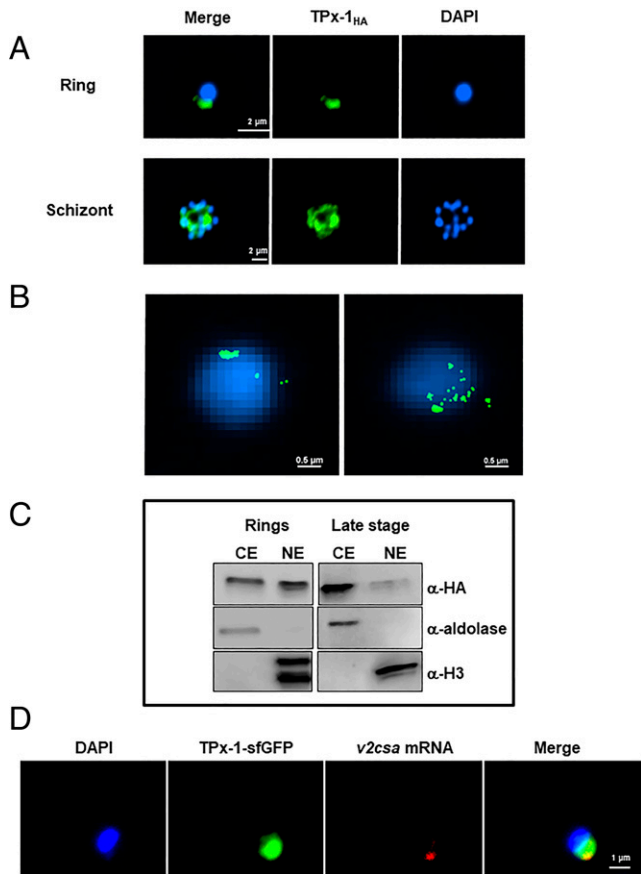
Fig. 3. *Pf*TPx-1 is localized to the active *var* expression site in ring-stage parasites. (*A*) Immunofluorescence microscopy of *Pf*TPx-1, endogenously tagged with HAx3 in ring (*Upper*) and schizont (*Lower*) parasites. Nuclei are stained with DAPI. (Scale bar, 2 μm.) (*B*) Superresolution STORM imaging of tightly synchronized ring-stage parasites (~18 h postinfection) expressing *Pf*TPx-1HAx3. Nuclei stained with YOYO1 were imaged by conventional epifluorescence for cellular orientation. (Scale bar, 0.5 μm.) (*C*) Cellular fractionation of synchronized ring and late-stage parasites was performed on the *Pf*TPx-1HAglmS line and nuclear and cytoplasmic extracts (NE and CE, respectively). *Pf*TPx-1 was detected with anti-HA, antialdolase was used as a cytoplasmic marker, and antihistone H3 as a nuclear marker. (*D*) RNA-FISH, of *var2csa*-expressing parasites that episomally express sfGFP-PfTPx-1 fusion (green), using custom-designed Stellaris probes that hybridize to *var2csa* (red). In all nuclei (*n* = 111) *Pf*TPx-1 was found to overlap with the active *var* mRNA. (Scale bar, 1 μm.)

entire *var* gene family by RT-qPCR (34) over time to detect changes caused by *Pf*TPx-1 overexpression. The initial C3 culture displayed heterogeneous *var* gene expression with no dominant *var* gene being transcribed in the parasite population (Fig. 6 *A*, *Top*, and *SI Appendix*, Fig. S9*B*). After the transfected parasite lines were established by selection with 2 μg/mL blasticidin, we performed RT-qPCR to obtain a baseline *var* transcription profile (Fig. 6), since transfection presents a bottleneck where *var* gene expression could change simply due to isolation of subpopulations from the original culture. The amount of blasticidin in the media was then increased to 10 μg/mL and RNA samples of ring-stage parasites were collected after 3 wk and 3 mo. We noticed that over time there was a gradual shift toward expression of *var2csa* in the line overexpressing *Pf*TPx-1, while *var2csa* levels remained low in the GFP overexpression control (11.2% vs. 2.5% at 3 wk and 24.3% vs. 2% at 3 mo) (Fig. 6*A* and *SI Appendix*, Fig. S9 *C and D*). Both the original culture and the GFP control exhibited *var* gene switching, as is typical for a heterogenous culture, but the rate of *var2csa* activation remained low compared to the *Pf*TPx-1 overexpression line (Fig. 6 and *SI Appendix*, Fig. S9 *B and C*). This result suggests that overexpression of *Pf*TPx-1 leads

to transcriptional changes that cause parasites within the population to switch to *var2csa* at an accelerated rate.

***Pf* TPx-1 Colocalizes with *Pf* SAMS in the Nucleus of Ring-Stage Parasites.** Accelerated activation of *var2csa* upon *Pf* TPx-1 overexpression is similar to a phenotype previously observed when a dominant–negative version of the histone methyl-transferase *Pf* SET2 was overexpressed (35). Histone methylation requires a constant supply of methyl groups, primarily supplied by the methyl donor, S-adenosylmethionine (SAM). *Pf* TPx-1 has been shown to interact with enzymes involved in SAM metabolism in vitro, including SAM-synthetase (SAMS) (PF3D7_0922200) (8, 10), and has experimentally been shown to act as an oxidoreductase and enhance SAMS activity in vitro (36). Although SAM is needed for DNA and RNA methylation in the nucleus, SAM metabolism is generally thought to take place in the cytoplasm. To test whether the nuclear *Pf* TPx-1 found at the *var* expression site could possibly interact with SAMS in the nucleus, we transfected a plasmid expressing *Pf* SAMS-3 X MYC into the transgenic *Pf* TPx-1$_{HA-glmS}$ line. By IFA, we found that *Pf* SAMS localized to a distinct region on the nuclear periphery in ring-stage parasites and showed partial overlapping occupancy with *Pf* TPx-1 (Fig. 7*A*). Nuclear localization of *Pf* SAMS was confirmed by cellular fractionation (Fig. 7*B*). The proximity of *Pf* TPx-1 to *Pf* SAMS in the nucleus in ring-stage parasites suggests that they may act together at the *var* expression site to epigenetically regulate *var* gene expression. Interestingly, when we overexpressed *Pf* SAMS in the *Pf* TPx-1 line, *var2csa* was activated, similar to the phenotype observed when *Pf* TPx-1 was overexpressed (Fig. 7*C*). This similarity further supports the idea that *Pf* TPx-1 may be recruited to the active *var* gene to support optimal redox conditions for *Pf* SAMS enzymatic activity that appears to be important for epigenetic regulation.

PfTPx-1 Knockdown Causes Transcriptional Changes of Several Gene Subsets. To look at the global transcriptional changes caused by *Pf* TPx-1 down-regulation, RNA sequencing (RNA-seq) was performed on tightly synchronized late ring stages of the DC-J line and a clone of the *Pf* TPx-1$_{HAglmS}$ line grown in the absence or presence of 5 mM GlcN for 96 h. Performing this comparison two cycles after knockdown, at late ring stages when *Pf* TPx-1 is mostly nuclear, maximizes our ability to potentially detect both primary and secondary transcriptional changes. We found that *Pf* TPx-1 mRNA levels were 3.5-fold down-regulated in the *Pf* TPx-1$_{HAglmS}$ compared to the parent DC-J line, and 78-fold down-regulated upon GlcN treatment (Fig. 8). We ensured that the RNA-seq data from all samples corresponded to hour 16 of the cell cycle, indicating that any differences observed are due to the treatment condition (GlcN/*Pf* TPx-1 knockdown) and not due to differences in cell-cycle timing. Our analysis indicated that there are few transcriptomic differences between DC-J and *Pf* TPx-1$_{HAglmS}$ growing on regular media (Fig. 8*B*); however, upon *Pf* TPx-1 knockdown (+GlcN), 692 transcripts were significantly changed (P_{adj} < 0.05) by at least twofold as compared to the DC-J control grown on GlcN (Fig. 8*C*). Strikingly, 91% (632 of 692) of these transcripts were down-regulated and only 9% were up-regulated, indicating that *Pf* TPx-1 may function as a nuclear factor that is involved in providing the optimal conditions for transcriptional activation. Our data showing that *Pf* TPx-1 is present in the part of the nucleus where active transcription takes place is in line with this observation. The up-regulated genes consisted primarily of genes from multicopy gene families (*Pf* EMP-1, stevor, rifins, *Pf* MC-2TM), which are often distinct between two clonal populations. Despite
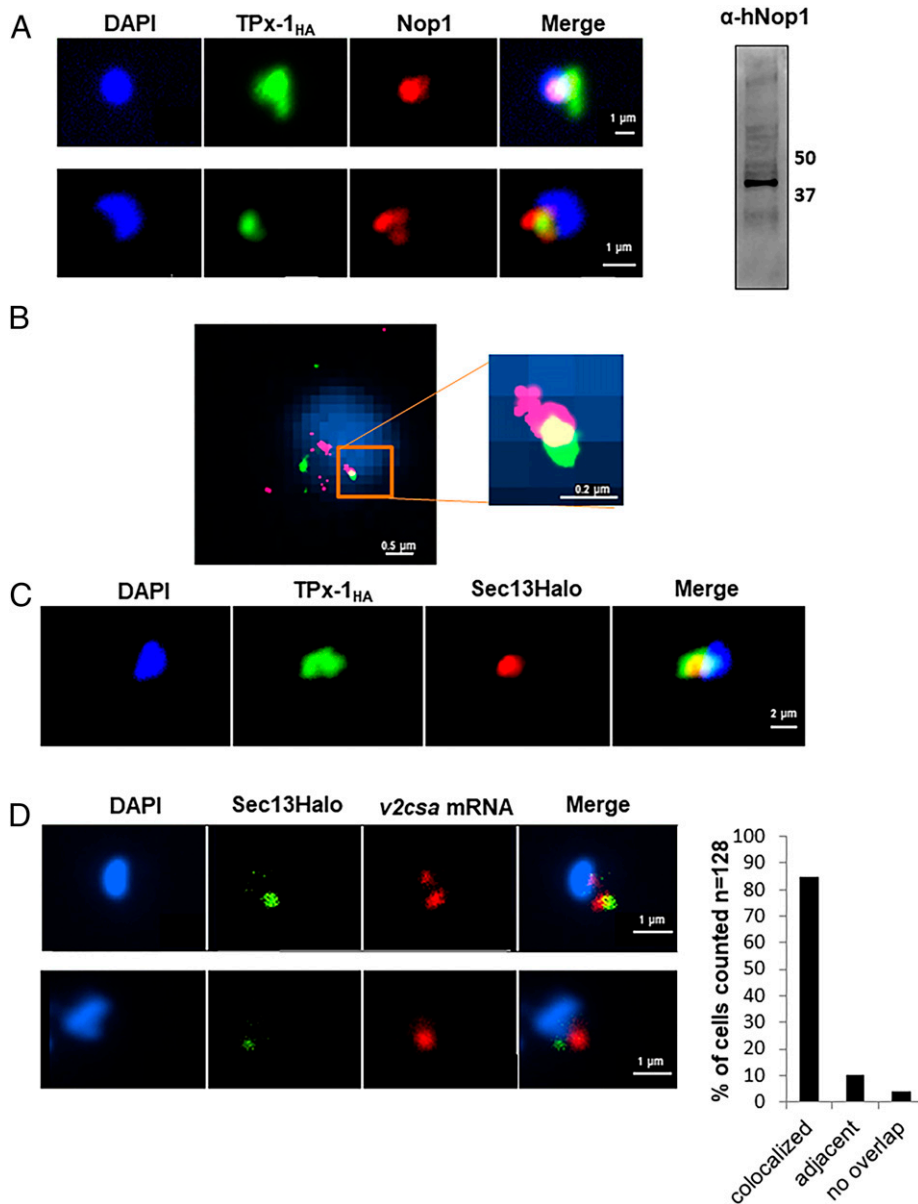
Fig. 4. *Pf*TPx-1 localizes to a transcriptionally active nuclear region in ring-stage parasites. (*A, Left*) Immunofluorescence microscopy of *Pf*TPx-1HAglms parasites where *Pf*TPx-1 (green) is associated with the nucleolar protein, *Pf*Nop1 (red). Nuclei are stained with DAPI. (Scale bar, 1 μm.) (*Right*) An anti hNop1/Fibrillarin antibody specifically detects *Pf*Nop1 in parasite extract. (*B*) Superresolution STORM imaging of *Pf*TPx-1 (green) and PfNop1 (red) in synchronized ring-stage *Pf*TPx-1HA parasites. Nuclei stained with YOYO1 were imaged by conventional epifluorescence for cellular orientation. An area of overlap is enlarged (square *Inset*). (Scale bar, 0.5 and 0.2 μm, respectively.) (*C*) Immunofluorescence of ring-stage *Pf*TPx-1HAglms (*Pf*TPx-1 in green) transfected with a Sec13-Halo plasmid (red). (Scale bar, 2 μm.) (*D*) RNA-FISH of CSA expressing parasites that carry a Sec13-Halo plasmid (green). RNA-FISH was performed using custom-designed Stellaris probes that hybridize to *var2csa* transcripts (red). Representative images of colocalized signals (*Upper*) and adjacent signals (*Lower*) are shown. (Scale bar, 1 μm.) Quantification of signals ($n = 128$) that were found to be overlapping or adjacent to each other are shown to the right.

the almost 80-fold reduction in *Pf*TPx-1 transcript, the resulting down-regulation of other transcripts was more modest (average 3.24-fold down-regulation, range $\log_2$fold -10 to -1), yet significant. Gene ontology and metabolic pathway enrichment analysis of down-regulated genes showed significant enrichment in the categories of nucleotide biosynthesis, mitochondrial electron transport, DNA binding and replication, and oxidoreductase activity (*SI Appendix*, Fig. S10). Overall, these data suggest that *Pf*TPx-1 is needed for transcriptional activation of particular gene subsets.

Discussion

The *var* antisense lncRNA transcripts were previously shown to be involved in *var* gene activation (5); however, the mechanism is unknown. In this study, we provide evidence that these lncRNAs are located at the *var* expression site, in close proximity to the nascent *var* mRNA, and that they are held in place by DNA:RNA interactions. These transcripts contain a hypervariable sequence that can confer gene specificity by marking a single gene for activation, while the conserved intronic sequence could be involved in an activation mechanism common to the entire *var* gene family. Indeed, in our dChIRP analysis, the majority of

protein–RNA interactions were obtained with the conserved part of the *var* lncRNA, while histones were the primary proteins pulled down with the gene-specific sequence of the lncRNA. These data support our observation that the lncRNA is anchored by DNA:RNA interactions and is incorporated into chromatin (5). Therefore, it is reasonable to suggest a model by which the gene-specific sequence of the antisense transcript marks the locus by forming a DNA:RNA hybrid, while the conserved region is involved in protein recruitment. lncRNAs can mediate transcriptional and epigenetic changes by recruiting transcriptional activators or chromatin-modifying enzymes (6). We further used the conserved region of the antisense lncRNA as bait and identified the proteins that interact with these transcripts. The *var* lncRNA interactome contained DNA/RNA binding proteins, such as Alba3/4 and polyadenylate binding protein, which have previously been mapped to *var* gene loci (37, 38), validating our methodologies. However, while it is well established that *var* genes are epigenetically regulated (39), we did not pull down any histone modifiers. Such interactions could be transient, or alternatively histone modifiers may act later in the cell cycle when the epigenetic imprint for the next cycle is needed (37). Though *Pf*TPx-1 was previously believed to be cytoplasmic, we consistently observed its
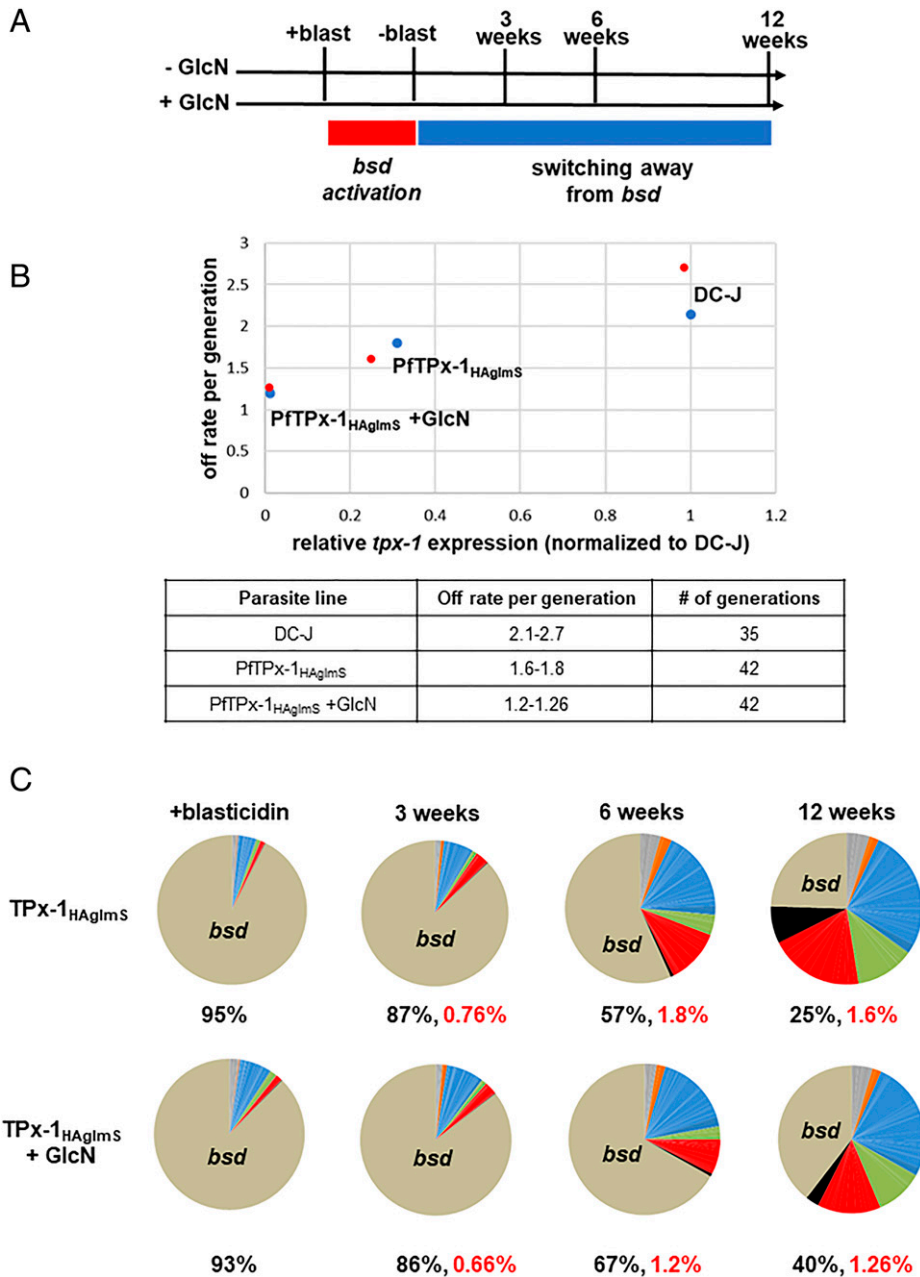
Fig. 5. *Pf*TPx-1 is involved in *var* gene switching. (*A*) Schematic of experimental design. Parasites were grown in the absence or presence of 5 mM glucosamine for the duration of the experiment (±GlcN). Blasticidin was added continuously for 3 wk to induce switching to the *var-bsd* (+blast, red rectangle). Blasticidin was then removed from the cultures to monitor switching away from *var-bsd* (−blast, blue rectangle). Parasites were collected 3, 6, or 12 wk following blasticidin removal. Synchronous ring-stage parasite (20 to 22 h postsynchronization) cultures were collected for RNA, and RT-qPCR for the *var* gene family was performed on cDNA at the times indicated. (*B*) Off switch rates per generation were calculated and plotted against the relative *Pf*TPx-1 mRNA levels of the different parasite lines. The results of the two biological replicates are shown in blue or red dots. The ranges of the calculated switch rates per generation, for each of the parasite lines, are presented in the lower table. (*C*) Dynamics in *var* switching patterns over time measured by RT-qPCR. Each pie graph represents the total of *var* gene transcripts with each slice of the pie representing the abundance of an individual *var* gene within the pool of *var* transcripts. The percentage of *bsd* transcript present in the total *var* gene pool is written below each pie graph and the off rate of *bsd* is written in red.

association with *var* lncRNAs within the nucleus. While it is difficult to discriminate between direct RNA–protein interaction or via protein complexes, using affinity chromatography and dChIRP, our RNA-EMSA on recombinant *Pf*TPx-1 supports direct interaction. Similarly, TPx-1 from humans (40) and *Plasmodium knowlesi* (*Pk*TPx-1), exhibits DNA and RNA binding in vitro, and *Pk*TPx-1 was shown to be able to melt an RNA stem-loop structure upon binding and act as an RNA chaperone (41), indicating that *Pf*TPx-1 might also be involved in molecular mechanisms in the nucleus that influence gene expression.

Interestingly, down-regulation of endogenous *Pf*TPx-1 slowed the *var* switch rate, while its overexpression accelerated activation of *var2csa*. *var2csa* is unique among the *var* gene family; it is highly conserved among different isolates and has an upstream open reading frame, which leads to its translational repression (42). Due to its conserved sequence and translational control, *var2csa* could be the ideal switch intermediate; *var2csa* is present in all parasite isolates and its activation would not necessarily initiate an immune response. This hypothesis is supported

by studies that observed selective activation of *var2csa* when *var* switching was induced through inhibition of histone modifiers (35, 43), as well as computational modeling that identified an important role for a common switch intermediate (or "sink node"), a function that could be fulfilled by *var2csa* (35, 44). In our experiments *Pf*TPx-1 was constitutively overexpressed and caused *var2csa* to remain activated for long periods, rather than the transient activation that would be predicted for a switch intermediate during a natural infection.

Activation of *var2csa* was previously reported upon overexpression of a dominant–negative *Pf*SET2 construct and treatment with the histone methyltransferase inhibitor chaetocin (35, 43), like the phenotype observed here when *Pf*TPx-1 is overexpressed. In addition, overexpression of SAM synthase (*Pf*SAMS) resulted in *var2csa* activation similar to overexpression of dominant–negative *Pf*SET2 and *Pf*TPx-1. However, *var2csa* activation occurred more rapidly when *Pf*SAMs is overexpressed possibly because SAMS enzymatic activity is the limiting factor for providing the methyl groups essential for *var2csa*
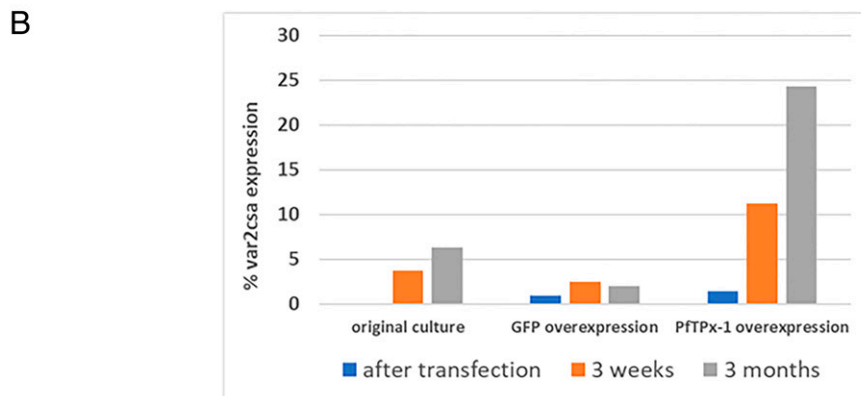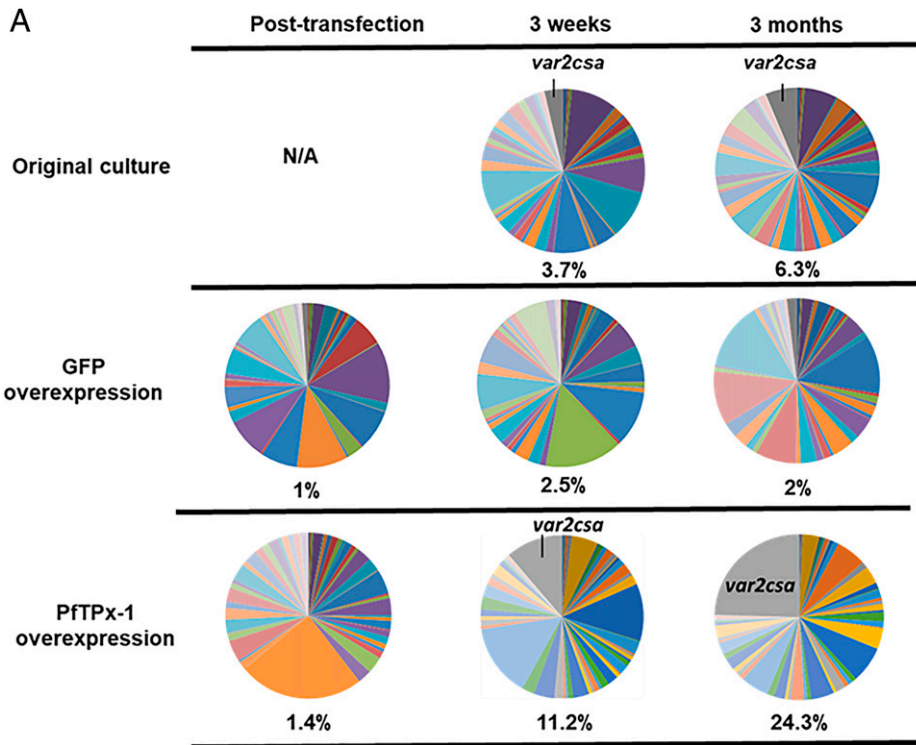
Fig. 6. *Pf*TPx-1 overexpression induces activation of *var2csa*. (*A*) *var* gene-expression profiles were determined by RT-qPCR for each culture posttransfection at low levels of PfTPx-1 or GFP (control) overexpression and then 3 wk and 3 mo after increasing levels of overexpression by increasing the dose of blasticidin from 2 to 10 µg/mL. *var* gene expression was also determined from the original parent culture, C3, at 3 wk and 3 mo in culture. Each pie graph represents the total of *var* gene transcripts with each slice of the pie representing the abundance of an individual *var* gene within the pool of *var* transcripts. The percentage of *var2csa* transcript present in the total *var* gene pool is written below each pie graph. (*B*) Quantification of the percentage of *var2csa* transcript within the total *var* transcript pool for each parasite population.

activation. Here we show that *Pf*TPx-1 and *Pf*SAMS occupy a subnuclear compartment where active transcription takes place. The nuclear localization of *Pf*SAMS may provide the methyl groups necessary for nearby histone methyltransferases to epigenetically mark their target genes. Several histone methylation marks are implicated in the epigenetic regulation of *var* gene expression (39). H3K36me3 is present at both active and silent *var* loci (35, 43), while H3K9me3 is found only at silent members of variant gene families and serves to recruit *Pf*HP1 (45–47). H3K4me3, on the other hand, is only present at the active *var* gene and is thought to be responsible for keeping the active *var* poised for the next cell cycle (37). Interestingly, in model organisms the histone methyltransferase that deposits H3K4me3 is sensitive to fluctuations in SAM levels (48). Studies have shown that cellular metabolism can influence gene expression via changes in histone methylation (49). In view of the interaction between *Pf*SAMS and *Pf*TPx-1 (10), the demonstrated role of *Pf*TPx-1 on the enzymatic activity of *Pf*SAMS (8), and their colocalization in the nucleus, it is possible that *Pf*SAMS and *Pf*TPx-1 play a role in providing methyl groups to methyltransferases at a specific nuclear subcompartment to influence gene expression.

The nuclear localization of *Pf*TPx-1 supports its association with transcriptional activity. It appears to reside in a perinuclear region that contains the *var* expression site, a portion of the nucleolus defined by Nop1, and the NPC marked by the nucleoporin *Pf*Sec13. The association of the *var* expression site with the NPC, as demonstrated here, is contrary to a previous report that used an antibody raised against a *Plasmodium* protein (PF3D7_1473700) that shares sequence similarity to the yeast *Sc*Nup116 (34% identity, 50% similarity), that did not colocalize with the *var* expression site (50). It remains to be determined whether the identified *P. falciparum* Nup116 is a bona fide nucleoporin. Interestingly, Nup116 is absent from *Plasmodium berghei* and is the only known putative nucleoporin that is not conserved among the different *Plasmodium* species (51). The spatial positioning of the *var* active site near the nuclear pore is in agreement with what is known from many model organisms and may contribute to efficient nuclear export of the *var* mRNA (28, 29).

In vivo *var* expression switching is postulated to occur in response to the adaptive immune attack against the expressed *Pf*EMP1 variant. However, the mechanistic process that governs such switching is not understood. Immune complexes
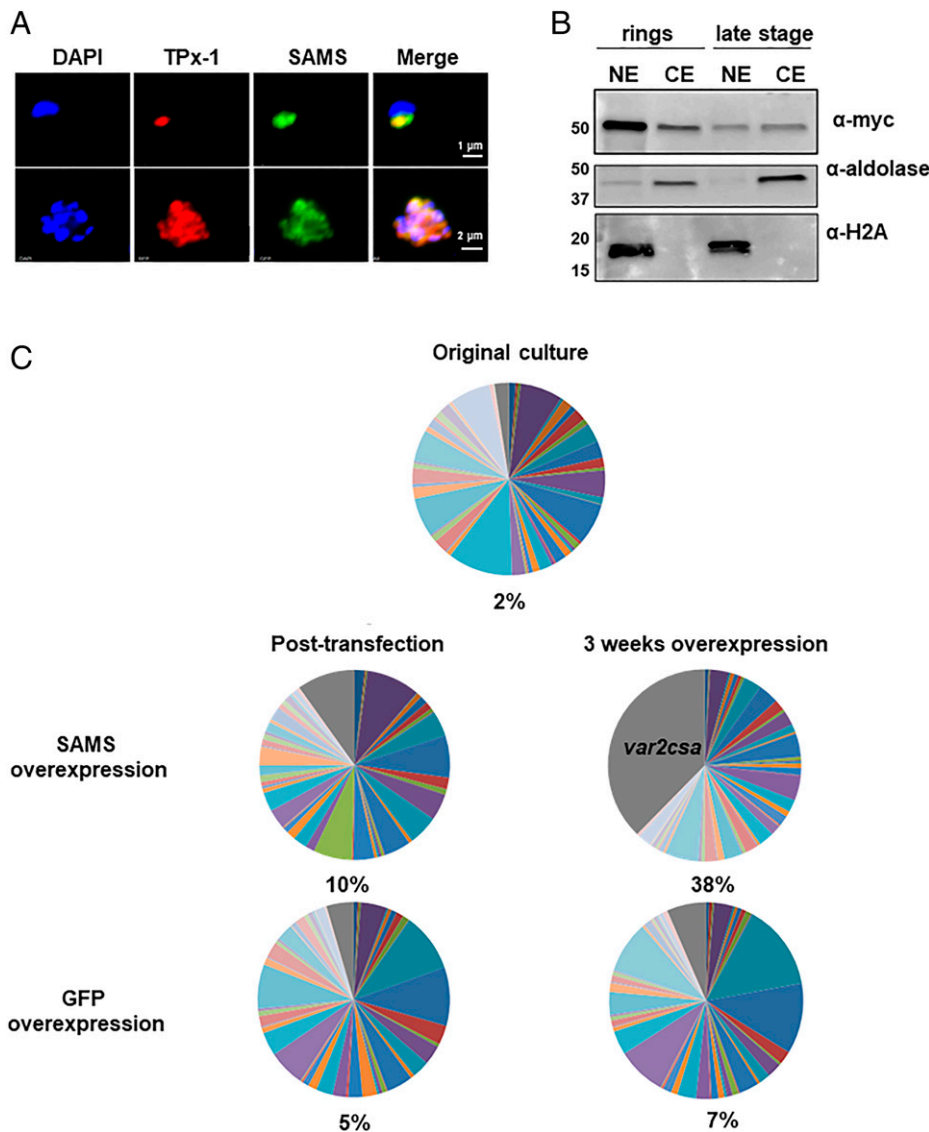
Fig. 7. *Pf*TPx-1 colocalizes with *Pf*SAMS in the nucleus of ring stage parasites. (*A*) Immunofluorescence microscopy of *Pf*TPx-1HAglmS parasites (*Pf*TPx-1 in red) transfected with a plasmid expressing *Pf*SAM-synthetase with a mycx3 tag (green) in ring (*Upper*) and schizont (*Lower*) parasites. Nuclei are stained with DAPI. (Scale bar, 1 μm.) (*B*) *Pf*SAMS is primarily nuclear in ring-stage parasites. Cellular fractionation of synchronized ring- and late-stage parasites was performed and the nuclear and cytoplasmic extracts (NE and CE, respectively) were subjected to Western blot analysis. *Pf*SAMS was detected using anti-myc antibody; antialdolase antibody was used to confirm cytoplasmic extraction, while antihistone H2A was used as a nuclear marker. (*C*) *var* gene-expression profiles were determined by RT-qPCR for *Pf*TPx-1HAglmS ring-stage parasites overexpressing *Pf*SAMS or GFP control after 1 mo of overexpression (5 μg/mL blasticidin). The percentage of *var2csa* transcript present in the total *var* gene pool was calculated and is written below each pie graph.

consisting of antibody–antigen pairs are powerful stimulators of immune cells, which can release a burst of ROS (52, 53). Interestingly, we observed an increase in *Pf*TPx-1 expression following exposure to different sources of oxidative stress (*SI Appendix,* Fig. S11) suggesting that *Pf*TPx-1 can sense and respond to stress conditions present in a human infection. It has been demonstrated that peroxiredoxins act as sensors that influence activities of their target proteins based on the cell's redox status (22, 54), and it is tempting to suggest that *Pf*TPx-1 could mediate transcriptional changes in response to changing environmental conditions and immune response.

While cellular metabolism is generally thought to occur outside the nucleus, the presence of nuclear metabolic enzymes is now widely accepted. Many of these enzymes function both in their canonical metabolic role and also take on additional roles in transcriptional regulation, providing a way for organisms to adapt their transcriptional program in response to metabolic stress (55). Therefore, it is not surprising that metabolic enzymes were found in the *var* lncRNA interactome. The recently published *var* interactome, using CRIPSR-dCas9 to target both active and silent *var* genes, also uncovered metabolic enzymes associated with *var* genes (38). Intriguingly, four glycolytic enzymes (Table 1) were found to interact with the nuclear *var* lncRNA. One of the main products

of glycolysis is NADH/NAD$^+$, which is impermeable to the nuclear membrane. Since many transcription factors require NADH to function, nuclear production of NADH is linked to transcriptional control (55). Interestingly, the NAD$^+$-dependent histone deacetylases, *Pf*Sir2a and *Pf*Sir2b, have been implicated in heterochromatin formation and *var* gene silencing (56, 57), although their functions may be strain-dependent (58). Aside from their canonical roles, in other organisms, glycolytic enzymes were shown to have noncanonical functions in the nucleus participating in transcription, DNA replication, and telomere maintenance (59). Interestingly, some of these glycolytic enzymes were also shown to interact with *Pf*TPx-1, suggesting that their functions may be redox-controlled (10). In addition, OAT was present in all three pull-down methodologies and has previously been shown to interact with *Pf*TPx-1 (8). Although there are reports of OAT being present in the nucleus in other organisms (60), to the best of our knowledge the nuclear roles of OAT are still elusive.

In conclusion, *Pf*TPx-1's association with *var* lncRNAs and its presence, adjacent to *Pf*SAMS, in the transcriptionally active region of the nucleus, provides a mechanistic clue as to how the parasite may sense and react to the changing conditions within the human host and switch *var* gene expression in response to malaria progression and immune attack.
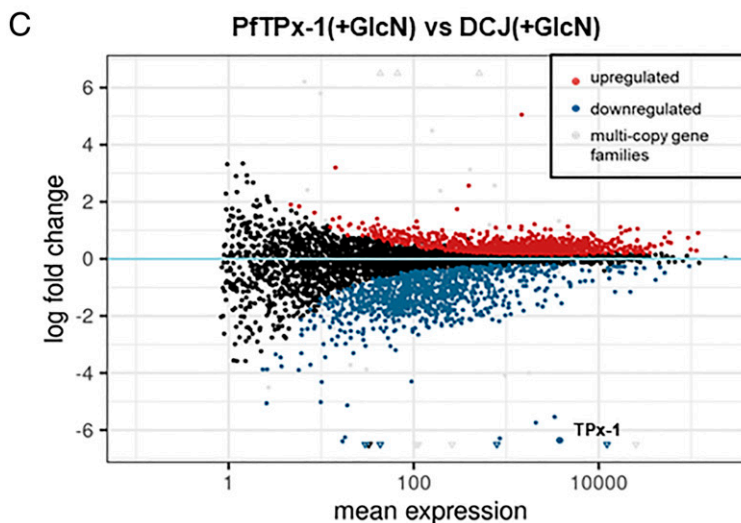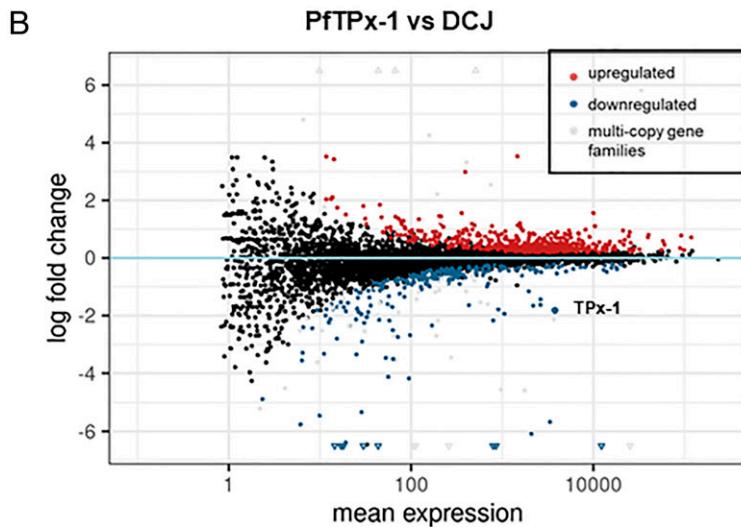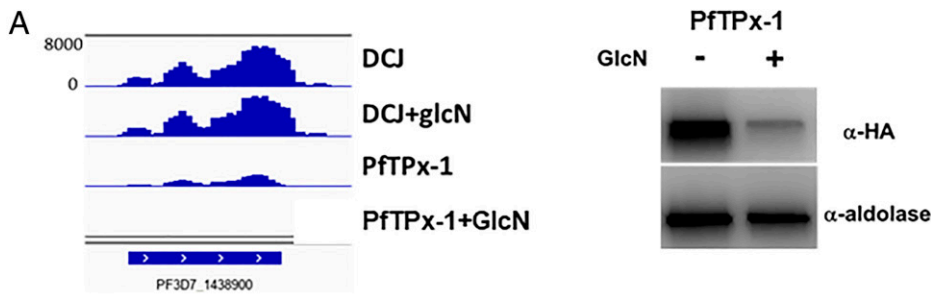
Fig. 8. *Pf*TPx-1 knockdown causes transcriptional changes of several gene subsets. (*A*) Expression profile for the *Pf*TPx-1 transcript (PF3D7_1438900) (bedgraph coverage illustration of relative expression from IGV) showing the knockdown of the *Pf*TPx-1 in the transgenic line compared to the parent DC-J line. Western blot analysis demonstrating the reduction of *Pf*TPx-1 protein levels in the transgenic lines are shown on the right. (*B* and *C*) MAplots of *Pf*TPx-1HAglmS vs. DC-J control without (*B*) and with GlcN (*C*), show genes that are differentially regulated upon down-regulation of *Pf*TPx-1 with GlcN. Within the plots, black dots represent nonsignificant genes. Significantly up-regulated and down-regulated genes ($P_{adj} < 0.05$) are shown in red and blue, respectively. Significantly changed genes of the multicopy gene families are shown in gray. Triangles are used to represent values that are beyond the axes limit.

Materials and Methods

Detailed materials and methods are found in the *SI Appendix*. Parasite culture, transfection, and selection was previously described (61–63). Genomic DNA extraction, RNA extraction, and cDNA synthesis were done as described previously (17, 64, 65). Transcript copy numbers was measured by RT-qPCR and were determined using the equation $2^{-\Delta\Delta CT}$ as described in the Applied Biosystems User Bulletin and previously published (17). TSA and Stellaris RNA FISH, nuclear fractionation, and affinity chromatography were performed as described previously with some modifications (66–68). Imaging analysis was performed using JACoP ImageJ plugin to calculate the Mander's overlap coefficient (69). dChIRP was performed as described previously (20, 21, 70). Probes were designed using Biosearch technologies Stellaris FISH Probe Designer. Probes were added to cross-linked and sonicated parasite samples, and after reverse cross-linking, protein samples were sent to LC-MS/MS. A detailed protocol can be found in *SI Appendix, Supplementary Methods*.

STORM imaging and analysis was performed as previously described (71). Calculation of off rate for individual *var* loci were calculated as previously described (32), where off rate is defined as the decrease of transcript from a particular *var* locus per generation. Parasite collection and RNA preparation for RNA-seq, as well as data analysis, is described in details in *SI Appendix*. Cell-cycle progression of our samples was normalized by comparing our RNA-seq data to Otto et al. (72). Significance threshold was taken as *P*adj < 0.05.

Data, Materials, and Software Availability. All study data are included in the article and supporting information.

1. (WHO) World Malaria Report 2020 (2020). https://www.who.int/publications/i/item/9789240015791. Accessed 31 July 2022.

2. T. D. Otto *et al.*, Long read assemblies of geographically dispersed *Plasmodium falciparum* isolates reveal highly structured subtelomeres. *Wellcome Open Res.* **3**, 52 (2018).

3. R. Dzikowski, K. W. Deitsch, Genetics of antigenic variation in *Plasmodium falciparum*. *Curr. Genet.* **55**, 103–110 (2009).

4. C. Epp, F. Li, C. A. Howitt, T. Chookajorn, K. W. Deitsch, Chromatin associated sense and antisense noncoding RNAs are transcribed from the var gene family of virulence genes of the malaria parasite *Plasmodium falciparum*. *RNA* **15**, 116–127 (2009).

5. I. Amit-Avraham *et al.*, Antisense long noncoding RNAs regulate var gene activation in the malaria parasite *Plasmodium falciparum*. *Proc. Natl. Acad. Sci. U.S.A.* **112**, E982–E991 (2015).

6. T. R. Mercer, M. E. Dinger, J. S. Mattick, Long non-coding RNAs: Insights into functions. *Nat. Rev. Genet.* **10**, 155–159 (2009).

7. S. Kawazu *et al.*, Molecular characterization of a 2-Cys peroxiredoxin from the human malaria parasite *Plasmodium falciparum*. *Mol. Biochem. Parasitol.* **116**, 73–79 (2001).

8. C. Brandstaedter *et al.*, The interactome of 2-Cys peroxiredoxins in *Plasmodium falciparum*. *Sci. Rep.* **9**, 13542 (2019).

9. M. Rahbari, S. Rahlfs, E. Jortzik, I. Bogeski, K. Becker, H_2O_2 dynamics in the malaria parasite *Plasmodium falciparum. PLoS One* **12**, e0174837 (2017).

10. N. Sturm *et al.*, Identification of proteins targeted by the thioredoxin superfamily in *Plasmodium falciparum. PLoS Pathog.* **5**, e1000383 (2009).

11. R. Kimura, K. Komaki-Yasuda, S. Kawazu, S. Kano, 2-Cys peroxiredoxin of *Plasmodium falciparum* is involved in resistance to heat stress of the parasite. *Parasitol. Int.* **62**, 137–143 (2013).

12. K. Yano *et al.*, Disruption of the Plasmodium berghei 2-Cys peroxiredoxin TPx-1 gene hinders the sporozoite development in the vector mosquito. *Mol. Biochem. Parasitol.* **159**, 142–145 (2008).

13. K. Yano *et al.*, 2-Cys peroxiredoxin TPx-1 is involved in gametocyte development in *Plasmodium berghei. Mol. Biochem. Parasitol.* **148**, 44–51 (2006).

14. K. Komaki-Yasuda, S. Kawazu, S. Kano, Disruption of the *Plasmodium falciparum* 2-Cys peroxiredoxin gene renders parasites hypersensitive to reactive oxygen and nitrogen species. *FEBS Lett.* **547**, 140–144 (2003).

15. R. Deslauriers, K. Butler, I. C. Smith, Oxidant stress in malaria as probed by stable nitroxide radicals in erythrocytes infected with *Plasmodium berghei*. The effects of primaquine and chloroquine. *Biochim. Biophys. Acta* **931**, 267–275 (1987).

16. K. Becker *et al.*, Oxidative stress in malaria parasite-infected erythrocytes: Host-parasite interactions. *Int. J. Parasitol.* **34**, 163–189 (2004).

17. R. Dzikowski, M. Frank, K. Deitsch, Mutually exclusive expression of virulence genes by malaria parasites is regulated independently of antigen production. *PLoS Pathog.* **2**, e22 (2006).

18. L. Jiang *et al.*, PfSETvs methylation of histone H3K36 represses virulence genes in *Plasmodium falciparum. Nature* **499**, 223–227 (2013).

19. I. Avraham, J. Schreier, R. Dzikowski, Insulator-like pairing elements regulate silencing and mutually exclusive expression in the malaria parasite *Plasmodium falciparum. Proc. Natl. Acad. Sci. U.S.A.* **109**, E3678–E3686 (2012).

20. J. J. Quinn *et al.*, Revealing long noncoding RNA architecture and functions using domain-specific chromatin isolation by RNA purification. *Nat. Biotechnol.* **32**, 933–940 (2014).

21. J. J. Quinn, H. Y. Chang, In situ dissection of RNA functional subunits by domain-specific chromatin isolation by RNA purification (dChIRP). *Methods Mol. Biol.* **1262**, 199–213 (2015).

22. L. E. Netto, F. Antunes, The roles of peroxiredoxin and thioredoxin in hydrogen peroxide sensing and in signal transduction. *Mol. Cells* **39**, 65–71 (2016).

23. S. Müller, Redox and antioxidant systems of the malaria parasite *Plasmodium falciparum*. *Mol. Microbiol.* **53**, 1291–1305 (2004).

24. J. Birnbaum *et al.*, A genetic system to study *Plasmodium falciparum* protein function. *Nat. Methods* **14**, 450–456 (2017).

25. P. Prommana *et al.*, Inducible knockdown of *Plasmodium* gene expression using the glmS ribozyme. *PLoS One* **8**, e73783 (2013).

26. S. C. Oehring *et al.*, Organellar proteomics reveals hundreds of novel nuclear proteins in the malaria parasite *Plasmodium falciparum*. *Genome Biol.* **13**, R108 (2012).

27. L. Mancio-Silva, Q. Zhang, C. Scheidig-Benatar, A. Scherf, Clustering of dispersed ribosomal DNA and its role in gene regulation and chromosome-end associations in malaria parasites. *Proc. Natl. Acad. Sci. U.S.A.* **107**, 15117–15122 (2010).

28. A. Akhtar, S. M. Gasser, The nuclear envelope and transcriptional control. *Nat. Rev. Genet.* **8**, 507–517 (2007).

29. G. Dieppois, F. Stutz, Connecting the transcription site to the nuclear pore: A multi-tether process that regulates gene expression. *J. Cell Sci.* **123**, 1989–1999 (2010).

30. N. Dahan-Pasternak *et al.*, PfSec13 is an unusual chromatin-associated nucleoporin of *Plasmodium falciparum* that is essential for parasite proliferation in human erythrocytes. *J. Cell Sci.* **126**, 3055–3069 (2013).

31. S. Kapishnikov *et al.*, Oriented nucleation of hemozoin at the digestive vacuole membrane in *Plasmodium falciparum. Proc. Natl. Acad. Sci. U.S.A.* **109**, 11188–11193 (2012).

32. M. Frank, R. Dzikowski, B. Amulic, K. Deitsch, Variable switching rates of malaria virulence genes are associated with chromosomal position. *Mol. Microbiol.* **64**, 1486–1498 (2007).

33. C. Epp, D. Raskolnikov, K. W. Deitsch, A regulatable transgene expression system for cultured *Plasmodium falciparum* parasites. *Malar. J.* **7**, 86 (2008).

34. A. Salanti *et al.*, Selective upregulation of a single distinctly structured var gene in chondroitin sulphate A-adhering *Plasmodium falciparum* involved in pregnancy-associated malaria. *Mol. Microbiol.* **49**, 179–191 (2003).

35. U. E. Ukaegbu *et al.*, A unique virulence gene occupies a principal position in immune evasion by the malaria parasite *Plasmodium falciparum*. *PLoS Genet.* **11**, e1005234 (2015).

36. J. Pretzel *et al.*, Characterization and redox regulation of *Plasmodium falciparum* methionine adenosyltransferase. *J. Biochem.* **160**, 355–367 (2016).

37. J. C. Volz *et al.*, PfSET10, a *Plasmodium falciparum* methyltransferase, maintains the active var gene in a poised state during parasite division. *Cell Host Microbe* **11**, 7–18 (2012).

38. J. M. Bryant *et al.*, Exploring the virulence gene interactome with CRISPR/dCas9 in the human malaria parasite. *Mol. Syst. Biol.* **16**, e9569 (2020).

39. K. W. Deitsch, R. Dzikowski, Variant gene expression and antigenic variation by malaria parasites. *Annu. Rev. Microbiol.* **71**, 625–641 (2017).

40. J. H. Kim *et al.*, RNA-binding properties and RNA chaperone activity of human peroxiredoxin 1. *Biochem. Biophys. Res. Commun.* **425**, 730–734 (2012).

41. H. Hakimi *et al.*, *Plasmodium knowlesi* thioredoxin peroxidase 1 binds to nucleic acids and has RNA chaperone activity. *Parasitol. Res.* **113**, 3957–3962 (2014).

42. B. Amulic, A. Salanti, T. Lavstsen, M. A. Nielsen, K. W. Deitsch, An upstream open reading frame controls translation of var2csa, a gene implicated in placental malaria. *PLoS Pathog.* **5**, e1000256 (2009).

43. U. E. Ukaegbu *et al.*, Recruitment of PfSET2 by RNA polymerase II to variant antigen encoding loci contributes to antigenic variation in *P. falciparum*. *PLoS Pathog.* **10**, e1003854 (2014).

44. M. Recker *et al.*, Antigenic variation in *Plasmodium falciparum* malaria involves a highly structured switching pattern. *PLoS Pathog.* **7**, e1001306 (2011).

45. C. Flueck *et al.*, *Plasmodium falciparum* heterochromatin protein 1 marks genomic loci linked to phenotypic variation of exported virulence factors. *PLoS Pathog.* **5**, e1000569 (2009).

46. J. J. Lopez-Rubio *et al.*, 5′ Flanking region of var genes nucleate histone modification patterns linked to phenotypic inheritance of virulence traits in malaria parasites. *Mol. Microbiol.* **66**, 1296–1305 (2007).

47. T. Chookajorn *et al.*, Epigenetic memory at malaria virulence genes. *Proc. Natl. Acad. Sci. U.S.A.* **104**, 899–902 (2007).

48. W. Ding *et al.*, Stress-responsive and metabolic gene regulation are altered in low S-adenosylmethionine. *PLoS Genet.* **14**, e1007812 (2018).

49. N. Shiraki *et al.*, Methionine regulates maintenance and differentiation of human pluripotent stem cells. *Cell Metab.* **19**, 780–794 (2014).

50. J. Guizetti, R. M. Martins, S. Guadagnini, A. Claes, A. Scherf, Nuclear pores and perinuclear expression sites of var and ribosomal DNA genes correspond to physically distinct regions in *Plasmodium falciparum*. *Eukaryot. Cell* **12**, 697–702 (2013).

51. J. Kehrer *et al.*, Nuclear pore complex components in the malaria parasite *Plasmodium berghei*. *Sci. Rep.* **8**, 11249 (2018).

52. S. Vermeren, U. Karmakar, A. G. Rossi, Immune complex-induced neutrophil functions: A focus on cell death. *Eur. J. Clin. Invest.* **48** (suppl. 2), e12948 (2018).

53. T. N. Mayadas, G. C. Tsokos, N. Tsuboi, Mechanisms of immune complex-mediated neutrophil recruitment and tissue injury. *Circulation* **120**, 2012–2024 (2009).

54. M. C. Sobotta *et al.*, Peroxiredoxin-2 and STAT3 form a redox relay for H_2O_2 signaling. *Nat. Chem. Biol.* **11**, 64–70 (2015).

55. A. E. Boukouris, S. D. Zervopoulos, E. D. Michelakis, Metabolic enzymes moonlighting in the nucleus: Metabolic regulation of gene transcription. *Trends Biochem. Sci.* **41**, 712–730 (2016).

56. L. H. Freitas-Junior *et al.*, Telomeric heterochromatin propagation and histone acetylation control mutually exclusive expression of antigenic variation genes in malaria parasites. *Cell* **121**, 25–36 (2005).

57. C. J. Merrick, M. T. Duraisingh, *Plasmodium falciparum* Sir2: An unusual sirtuin with dual histone deacetylase and ADP-ribosyltransferase activity. *Eukaryot. Cell* **6**, 2081–2091 (2007).

58. C. J. Merrick *et al.*, Functional analysis of sirtuin genes in multiple *Plasmodium falciparum* strains. *PLoS One* **10**, e0118865 (2015).

59. P. Huangyang, M. C. Simon, Hidden features: Exploring the non-canonical functions of metabolic enzymes. *Dis. Model. Mech.* **11**, dmm033365 (2018).

60. A. Ginguay, L. Cynober, E. Curis, I. Nicolis, Ornithine aminotransferase, an important glutamate-metabolizing enzyme at the crossroads of multiple metabolic pathways. *Biology (Basel)* **6**, E18 (2017).

61. S. B. Aley, J. A. Sherwood, R. J. Howard, Knob-positive and knob-negative *Plasmodium falciparum* differ in expression of a strain-specific malarial antigen on the surface of infected erythrocytes. *J. Exp. Med.* **160**, 1585–1590 (1984).

62. M. S. Calderwood, L. Gannoun-Zaki, T. E. Wellems, K. W. Deitsch, *Plasmodium falciparum* var genes are regulated by two regions with separate promoters, one upstream of the coding region and a second within the intron. *J. Biol. Chem.* **278**, 34125–34132 (2003).

63. K. Deitsch, C. Driskill, T. Wellems, Transformation of malaria parasites by the spontaneous uptake and expression of DNA from human erythrocytes. *Nucleic Acids Res.* **29**, 850–853 (2001).

64. R. Dzikowski, K. W. Deitsch, Active transcription is required for maintenance of epigenetic memory in the malaria parasite *Plasmodium falciparum*. *J. Mol. Biol.* **382**, 288–297 (2008).

65. S. Kyes, R. Pinches, C. Newbold, A simple RNA analysis method shows var and rif multigene family expression patterns in *Plasmodium falciparum*. *Mol. Biochem. Parasitol.* **105**, 311–315 (2000).

66. E. Ronander, D. C. Bengtsson, L. Joergensen, A. T. Jensen, D. E. Arnot, Analysis of single-cell gene transcription by RNA fluorescent in situ hybridization (FISH). *J. Vis. Exp.* **68**, 4073 (2012).

67. T. S. Voss, M. Mini, P. Jenoe, H. P. Beck, *Plasmodium falciparum* possesses a cell cycle-regulated short type replication protein A large subunit encoded by an unusual transcript. *J. Biol. Chem.* **277**, 17493–17501 (2002).

68. B. L. Jutras, A. Verma, B. Stevenson, Identification of novel DNA-binding proteins using DNA-affinity chromatography/pull down. *Curr. Protoc. Microbiol.*, Chapter 1: Unit1F.1 (2012).

69. S. Bolte, F. P. Cordelières, A guided tour into subcellular colocalization analysis in light microscopy. *J. Microsc.* **224**, 213–232 (2006).

70. C. Chu, J. Quinn, H. Y. Chang, Chromatin isolation by RNA purification (ChIRP). *J. Vis. Exp.* **61**, 3912 (2012).

71. Y. Fastman *et al.*, An upstream open reading frame (uORF) signals for cellular localization of the virulence factor implicated in pregnancy associated malaria. *Nucleic Acids Res.* **46**, 4919–4932 (2018).

72. T. D. Otto *et al.*, New insights into the blood-stage transcriptome of Plasmodium falciparum using RNA-Seq. *Mol. Microbiol.* **76**, 12–24 (2010).